AGU PUBLICATIONS

Supporting Information for

"Inferring the Shallow Layered Structure at the Chang'E-4 Landing Site: A Novel Interpretation Approach Using Lunar Penetrating Radar"

Iraklis Giannakis[1], Feng Zhou[2], Craig Warren[3], Antonios Giannopoulos[4]

[1]I. Giannakis is with the School of Geosciences, University of Aberdeen, Meston Building, Kings College, Aberdeen, UK, AB24 3FX. E-mail: iraklis.giannakis@abdn.ac.uk

[2]F. Zhou is with the China University of Geosciences (Wuhan), School of Mechanical Engineering and Electronic Information, Wuhan, China, 388 Lumo Rd, 430074. E-mail: zhoufeng@cug.edu.cn

[3]C. Warren is with the Department of Mechanical and Construction Engineering, Northumbria University, Newcastle, UK, NE1 8ST, E-mail: craig.warren@northumbria.ac.uk

[4]A. Giannopoulos is with the School of Engineering, The University of Edinburgh, Edinburgh, EH9 3FG, UK. E-mail: a.giannopoulos@ed.ac.uk

Contents of this file

February 5, 2021, 7:36pm

Introduction

The supporting information includes, Texts S1-S3 and Figures S1-S3. Text S1 describes the conventional hyperbola-fitting that is compared to the proposed interpretation tool. Texts S2 and S3 are the gprMax input files for the numerical models used in Section 3.2, Figure 2 in the manuscript. Figure S1 illustrates the framework within which conventional hyperbola fitting operates. Figure S2 illustrates the landing site for the Chang'E-4 mission and some info for the surrounding craters and the geological setup of the area. Figure S3 zooms in to the fitted hyperbolas subject to the layered model shown in Figure 3_A in the manuscript.

Text S1. Conventional Hyperbola-Fitting with Dix Conversion

Figure S1 illustrates the measurement configuration used in a typical hyperbola-fitting scenario. A cylindrical target with radius R is buried at an arbitrary point $\overrightarrow{A} = \langle x_0, d \rangle$, where x_0 and d are the X-ordinate and the depth at the centre of the target. The principal axis of the cylinder is assumed to be perpendicular to the line of measurements. The medium is a homogeneous half-space with relative permittivity ϵ, zero conductivity ($\sigma = 0$) and no magnetic properties ($\mu = 0$). The velocity within this medium is uniform and equals with $c = \frac{c_0}{\sqrt{\epsilon}}$, where $c_0 \approx 2.99 \times 10^8 m/s$ is the velocity of light in free space.

Subject to these constrains, it can be easily deducted that the time (t) of the first arrivals will form a hyperbola in the $t - x$ domain, described by

$$t = \frac{2}{c_0}\sqrt{\epsilon}\left(||\overrightarrow{A} - \overrightarrow{B}|| - R\right). \quad (1)$$

Notice that the depth d of the target can be calculted from the apex of the hyperbola $[x_0, t_0]$ in the measured radagram via

$$d = \frac{c_0 t_0}{2\sqrt{\epsilon}} + R. \tag{2}$$

Therefore, the only unknowns in equation (1) are the relative permittivity ϵ and the radius of the target R. Hyperbola-fitting tries to find the best set of ϵ and R that minimises the error $\min_{\epsilon,R} ||\mathbf{t} - \mathbf{T}||$ between the measured first arrivals $\mathbf{T} \in \mathbb{R}^n$ and the ones calculated using equation (1) $\mathbf{t} \in \mathbb{R}^n$, where n is the number of points used for the minimization. The minimization $\min_{\epsilon,R} ||\mathbf{t} - \mathbf{T}||$ is singular since they are multiple combinations of (R, ϵ) that fits the measured hyperbola (Mertens et al., 2016; Giannakis et al., 2019). To overcome this, the radius is assumed to be equal with zero $R = 0$, which implies, that hyperbola-fitting holds true for targets that are relatively small (compared to the scale of the model).

The above framework holds true for homogeneous half-spaces subject to relatively small targets. If the permittivity of a medium varies with depth (which is the most often scenario), then the estimated permittivity using hyperbola-fitting will correspond to the bulk permittivity from the free surface to the investigated target. The bulk permittivity can be mapped with respect to depth using different targets buried at different depths. The Dix conversion (Dix, 1955) is often used in order to transform the bulk permittivity to the actual permittivity (Dong et al., 2020)

$$V_{n+1} = \sqrt{\frac{v_{n+1}^2 t_{n+1} - v_n^2 t_n}{t_{n+1} - t_n}}, \tag{3}$$

where v_n is the average velocity at the time t_n.

Text S2. gprMax input file for Model 1, Figure 2

```
#domain: 1 2 0.005

#dx_dy_dz: 0.005 0.005 0.005

#time_window: 3000

#python:

import numpy as np

p0=[-187.5000, 212.5000, -60.0000, 10.0000]

nx=np.array([i/100 for i in range(0,80)])

nz=p0[0]*nx**3 + p0[1]*nx**2 + p0[2]*nx + p0[3]

for i in range(0,80):

        print("material: {} 0 1 0 {}".format(nz[i], i))

        print("box: {} {} {} {} {} {} {}".format(nx[i], 0, 0, nx[i]+0.01, 2, 0.005, i))

#end_python:

#material: 10 10 1 0 pp

#cylinder: 0.7 0.2 0 0.7 0.2 0.005 0.025 pp

#cylinder: 0.6 0.4 0 0.6 0.4 0.005 0.025 pp

#cylinder: 0.65 0.3 0 0.65 0.3 0.005 0.025 pp

#cylinder: 0.55 1 0 0.55 1 0.005 0.025 pp

#cylinder: 0.3 1.3 0 0.3 1.3 0.005 0.025 pp

#cylinder: 0.45 0.4 0 0.45 0.4 0.005 0.025 pp

#cylinder: 0.25 1 0 0.25 1 0.005 0.025 pp

#cylinder: 0.75 1.7 0 0.75 1.7 0.005 0.025 pp
```

```
#cylinder: 0.4 0.7 0 0.4 0.7 0.005 0.025 pp

#waveform: gaussiandot 1 1e9 mypulse

#hertzian_dipole: z 0.8 0.1 0 mypulse

#rx: 0.8 0.105 0

#src_steps: 0 0.02 0

#rx_steps: 0 0.02 0
```

Text S3: gprMax input file for Model 2, Figure 2

```
#domain: 1 2 0.005

#dx_dy_dz: 0.005 0.005 0.005

#time_window: 3000

#python:

import numpy as np

p0=[-37.5000,30.0000,2.0000]

nx=np.array([i/100 for i in range(0,80)])

nz=p0[0]*nx**3 + p0[1]*nx**2 + p0[2]*nx + p0[3]

for i in range(0,80):

    print("material: {} 0 1 0 {}".format(nz[i], i))

    print("box: {} {} {} {} {} {} {}".format( nx[i], 0, 0, nx[i]+0.01, 2, 0.005, i))

#end_python:

#material: 10 10 1 0 pp

#cylinder: 0.7 0.2 0 0.7 0.2 0.005 0.025 pp
```

#cylinder: 0.6 0.4 0 0.6 0.4 0.005 0.025 pp

#cylinder: 0.65 0.3 0 0.65 0.3 0.005 0.025 pp

#cylinder: 0.55 1 0 0.55 1 0.005 0.025 pp

#cylinder: 0.3 1.3 0 0.3 1.3 0.005 0.025 pp

#cylinder: 0.45 0.4 0 0.45 0.4 0.005 0.025 pp

#cylinder: 0.25 1 0 0.25 1 0.005 0.025 pp

#cylinder: 0.75 1.7 0 0.75 1.7 0.005 0.025 pp

#cylinder: 0.4 0.7 0 0.4 0.7 0.005 0.025 pp

#waveform: gaussiandot 1 1e9 mypulse

#hertzian_dipole: z 0.8 0.1 0 mypulse

#rx: 0.8 0.105 0

#src_steps: 0 0.02 0

#rx_steps: 0 0.02 0

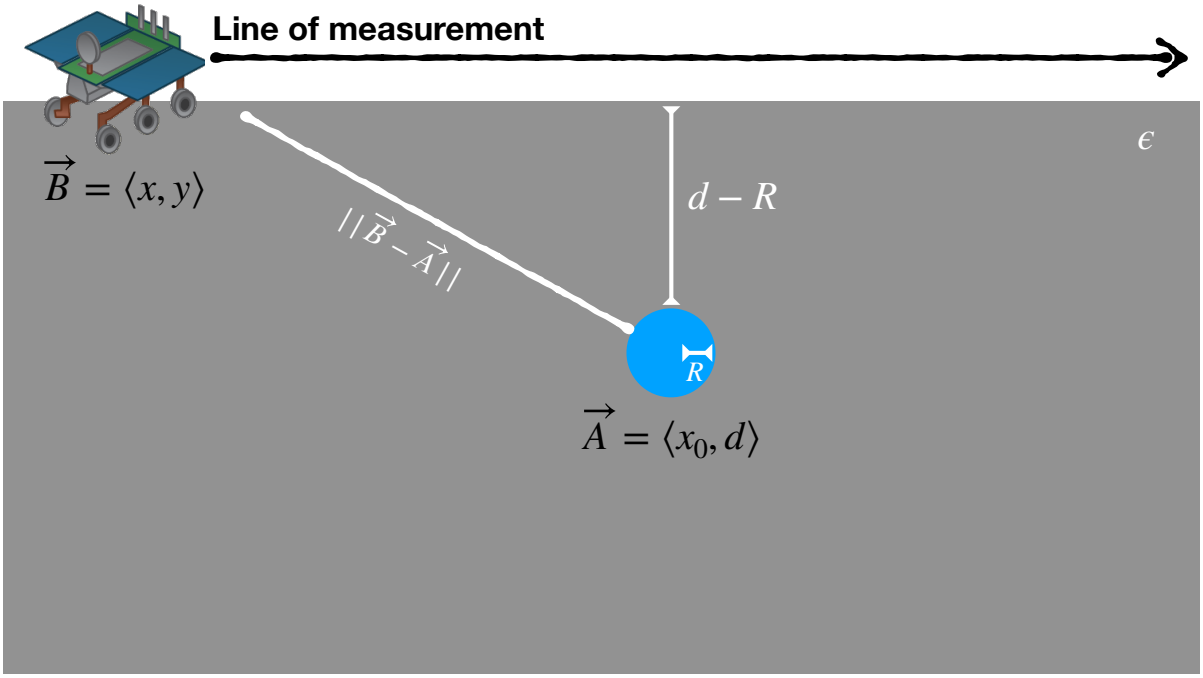

Figure S1. A typical hyperbola-fitting scenario with a cylindrical target with radius R buried in a homogeneous half-space with electric permittivity ϵ. The vector positions of the center of the target and the antenna are $\overrightarrow{A} = \langle x_0, d \rangle$ and $\overrightarrow{B} = \langle x, y \rangle$ respectively. The distance between the antenna and the surface of the target equals with $||\overrightarrow{A} - \overrightarrow{B}|| - R$.

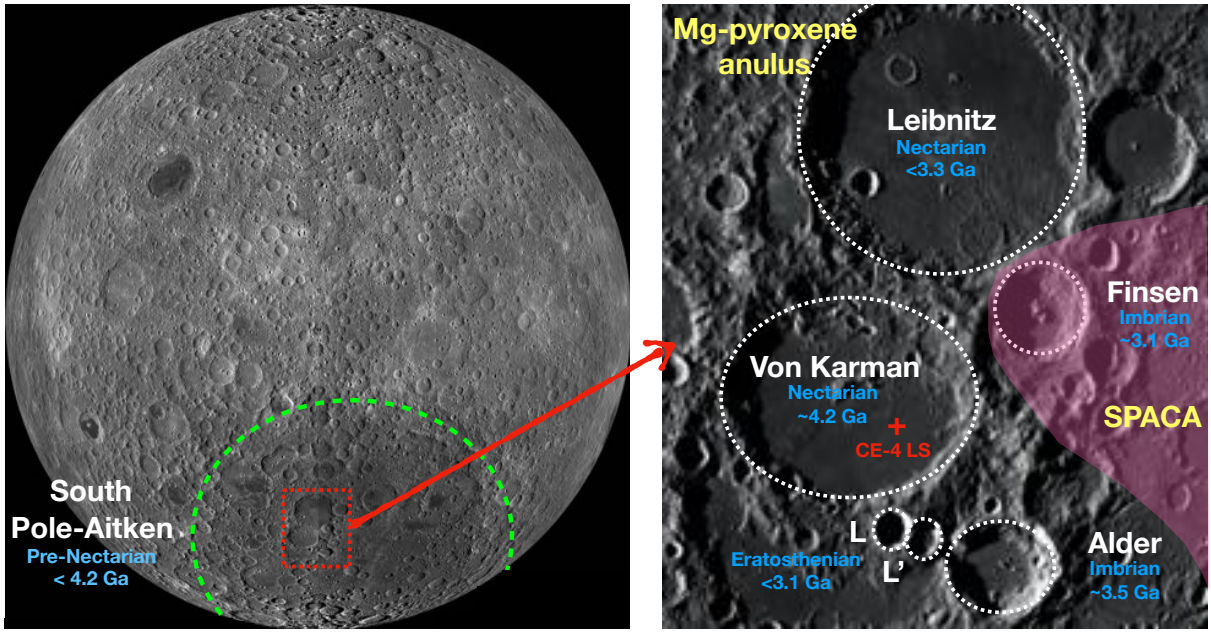

Figure S2. The Chang'E-4 landing site (CE-4 LS) –indicated with red cross– at Von Kármán (VK) crater at 44.45°S, 176.3°E. The Leibnitz crater (Nectarian age) has shaped the north part of the VK crater and provided the initial ejecta layer on top of the brecciated bedrock. VK crater was then flooded with basalts during Imbrium after the creation of Aldrer crater. During the late Imbrium and early Eratosthenian, the craters Finsen, VK L and L' were formed and provided the main ejecta materials on the top surface of VK. All the aforementioned craters are within the Mg-rich anulus while Finsen is at the SPACA zone (pink area). The dates are based on (Lu et al., 2021). The images are available from the Lunar Reconnaissance Orbiter's Wide Angle Camera. Image Credit: NASA, GSFC, Arizona State Univ. Lunar Reconnaissance Orbiter, available at `https://apod.nasa.gov/apod/ap161230.html`.

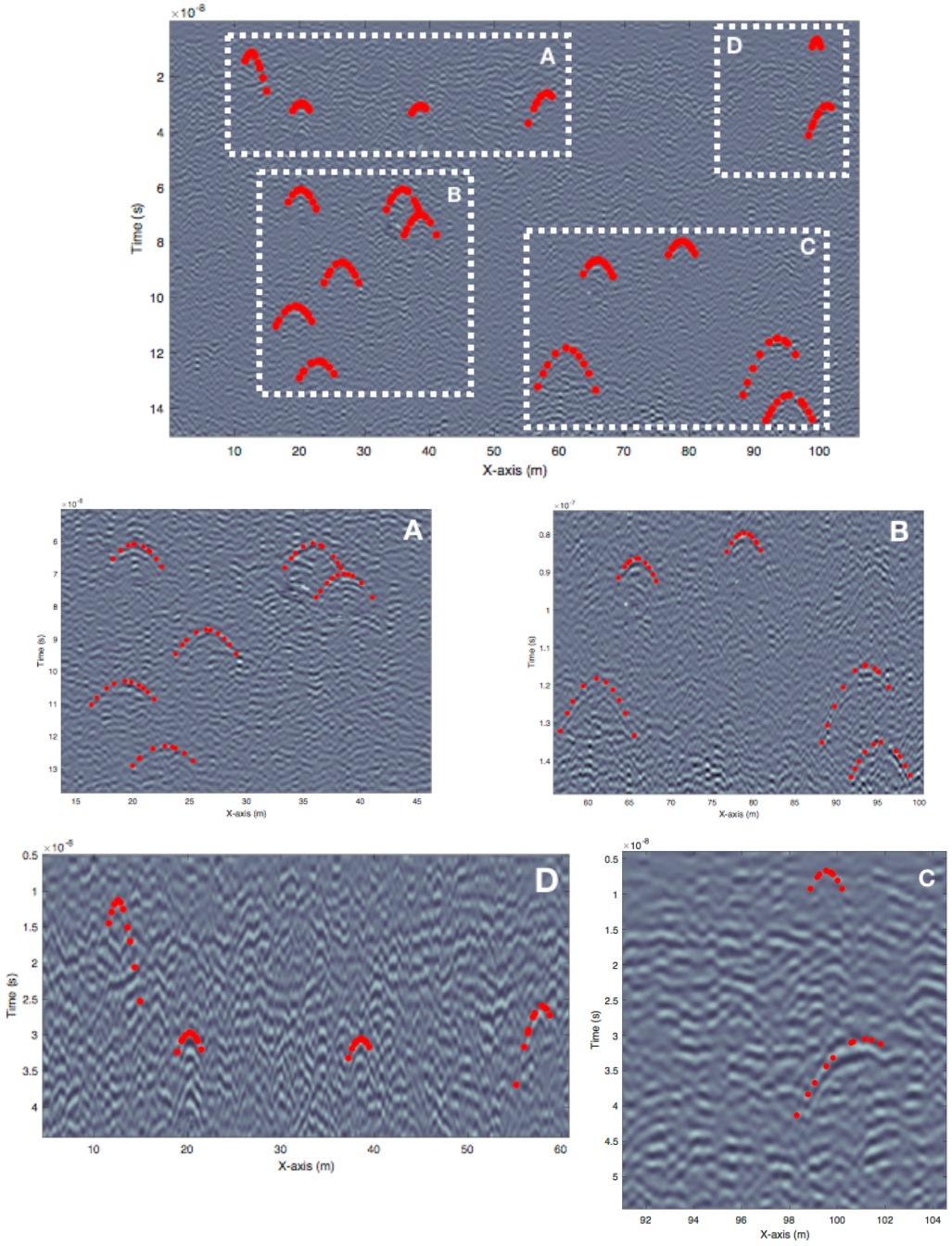

Figure S3. The processed B-Scan using the high frequency LPR antenna from the Yutu-2 rover. With red circles are the fitted hyperbolas for the layered structure illustrated in Figure 3_A in the manuscript. The Chang'E-4 Lunar Penetrating Radar data are available from the Data Publishing and Information Service System of China Lunar Exploration Program `http://moon.bao.ac.cn/searchOrder_dataSearchData.search`.

References

Dix, C. H. (1955). Seismic velocities from surface measurements. *Geophysics*, *20*, 68-86.

Dong, Z., Fang, G., Zhao, D., Zhou, B., Gao, Y., & Ji, Y. (2020). Dielectric properties of lunar subsurface materials. *Geophysical Research Letters*, *47*.

Giannakis, I., Giannopoulos, A., & Warren, C. (2019). A machine learning-based fast-forward solver for ground penetrating radar with application to full-waveform inversion. *IEEE Transactions on Geoscience and Remote Sensing*, *57*(7), 4417-4426.

Lu, Y., Wu, Y., Michael, G. G., Ma, J., Cai, W., & Qin, N. (2021). Chronological sequence of chang'e-4 landing zone within von kármán crater. *Icarus*, *354*, 114086.

Mertens, L., Persico, R., Matera, L., & Lambot, S. (2016). Automated detection of reflection hyperbolas in complex GPR images with no a priori knowledge on the medium. *IEEE Transactions on Geoscience and Remote Sensing*, *54*(1), 580-596.